COCrIP: Compliant OmniCrawler In-pipeline Robot

Akash Singh[1], Enna Sachdeva[1], Abhishek Sarkar[1], K.Madhava Krishna[1]

***Abstract*— This paper presents a modular in-pipeline climbing robot with a novel compliant foldable OmniCrawler mechanism. The robot has a series of 3 compliant foldable OmniCrawler modules interconnected by links via passive joints. The circular cross-section of the module enables a holonomic motion to facilitate the alignment of the robot in the direction of bends. Additionally, the crawler mechanism provides a fair amount of traction, even on slippery pipe surfaces. These advantages of crawler modules have been further augmented by incorporating active compliance in the module, which helps to negotiate sharp bends in small diameter pipes. Introducing compliance in the crawler module with a single chain-lugs assembly is the the key novelty of this design. For the desirable pipe diameter and curvature of the bends, the spring stiffness value for each passive joint is determined by formulating a constrained optimization problem using the quasi-static model of the robot. Moreover, a minimum friction coefficient value between the module-pipe surface which can be vertically climbed by the robot without slipping is estimated. The numerical simulation results have further been validated by experiments on real robot prototype.**

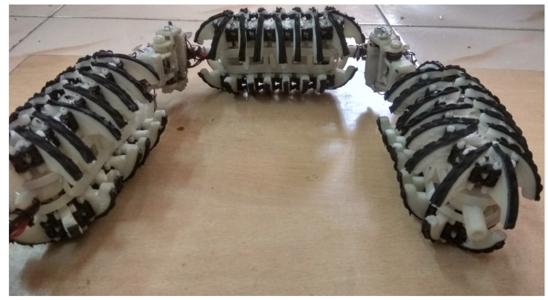

Fig. 1: Prototype of the Proposed Design

I. INTRODUCTION

In-pipeline climbing robots are highly favorable for non-destructive testing (NDT), inspection and maintenance of complex pipeline networks. Moreover, the widely spread oil and gas pipelines buried underneath the sea can only be accessed by a robot capable of overcoming bumps, sharp edged joints, valves and bends, while traversing. This has led various researchers and practitioners to design robots for small diameter complex pipe networks, since most of the industrial applications including power plants, boilers etc., as well as indoor applications deploy pipes of diameter smaller than 100mm.

A recent state of the art of wheeled, caterpillar, legged, inchworm, screw and Pipe Inspection Gauges (PIG) type pipeline robots is well documented in [1]. To primarily enhance the traveling performance and speed of locomotion in small diameter pipes, numerous multi-linked wheeled robots have been developed. Dertien.et.al [2] proposes an omnidirectional wheeled robot for in-pipe inspection (PIRATE) to overcome smooth bends. Hirose [3] proposed a 'PipeTron' series of multilink articulated snake-like robots with active wheels. PipeTron-I maintains a zig-zag posture to clamp in the pipe, by pulling a pair of steel wires that goes along its backbone and the differential tension in wires provides the twisting motion required to bend the robot. Further, in PipeTron-VII, twisting motion was realized by the differential speed of each driving wheel. Similarly, a series of Multifunctional Robot for IN-pipe inSPECTion (MRINSPECT) robot [4], [5], [6], [10] has been developed for a range of pipe diameters, where MRINSPECT IV [6] was specifically designed for pipelines of Ø4 inches. However, when its rear module loses contact with the pipe surface at T-junction, it fails to realize backward motion. All these articulated robots including [7], use passive clamping mechanism and hence use less number of actuators which simplifies the control strategy.

For small diameter pipelines, screw mechanism based robots have been designed with a further lesser number of actuators than in articulated robots. They have the advantage of achieving efficient helical motion inside pipes with simple transmission mechanism, using a single actuator for both driving and rolling motion. Hirose [8] designed 'Thes-II' robot by interconnecting multiple screw driving modules for Ø50 mm gas pipelines for long-distance locomotion. Atsushi [9] designed a screw driving robot using 2 actuators with one being used for both driving and rolling motion and the other one used to select pathways (for steering mode) in branched pipes. However, its unexpected mobility as a result of differential motion may not enable it to navigate autonomously in a known pipe environment.

The wheeled robot discussed so far indeed possess good maneuverability and steering abilities to overcome pipe bends. But they may get stuck on uneven pipe surface and experience the problem of wheel slip on low friction surface. Also, wheels may lack sufficient traction force for climbing on smooth and sticky surfaces. Though these problems have been overcome by designing a number of tank-like crawler robots [11], [12], the size of the crawler modules limits its ability to realize easy and efficient turning motion and steerability in bends. Kwon [11] addresses this

*This work was not supported by any organization

[1]All authors are with Robotics Research Center, IIIT-Hyderabad, Gachibowli-500032, India
akashvnit2016@gmail.com
sachdeva.enna@research.iiit.ac.in
abhishek.sarkar@iiit.ac.in
mkrishna@iiit.ac.in

problem by connecting a series of crawler modules, where collaborative control of modules enables steering motion in bends. Despite providing greater traction on low friction surfaces, conventional crawler modules sink into the soft surface while inclined [13]. Also, making a transition from bigger to smaller diameter and negotiating sharp turns in small diameter pipes become challenging in the conventional crawler pipeline robots.

This paper seeks to address these problems with the design of a modular Compliant OmniCrawler In-Pipeline climbing robot (COCrIP), shown in Fig.1. The design of the OmniCrawler module, inspired by [13], employs a series of lugs which results in a significant increase in the contact area and therefore, the traction between the lugs-pipe surface interface. The circular cross-section avoids a problem of the sinking of modules in a marshy surface, which makes it robust enough to crawl inside pipes with low friction coefficient values. The proposed design consists of three such modules interconnected by links with the passive compliant joints. The holonomic motion of the robot enables it to align itself in the direction of bends, beforehand. To negotiate sharp turns in small diameter pipes, each OmniCrawler module is further made compliant by incorporating active compliant joints, realized using series elastic actuators, in it. Instead of cascading multiple modules, the novelty of the proposed design lies in incorporating compliance in the crawler module itself, such that a chain-lugs assembly traverse over the module's chassis according to its bend configuration. The modularity of the robot eases its maneuverability with respect to variation in pipe diameter (transition from lower to higher as well as higher to lower diameters) and the compliance enables it to overcome sharp turns while deriving the advantages of OmniCrawler modules.

The organization of the paper is as follows. In Section II, a detailed description of the robot mechanism is discussed. Section III discusses various in-pipe traversal locomotion modes of the robot. Section IV discusses the optimization framework to estimate an optimal spring stiffness and the limiting value of friction coefficient between the pipe and the module surface, which the robot can climb vertically with the designed spring values. Furthermore, simulations and experimental results to validate the proof of concept of the mechanical design and mathematical formulation are given in Sections V and VI, respectively.

II. Mechanical Design Overview

The robot has a kinematic chain of 3 compliant foldable OmniCrawler modules with a link connected by a passive joint between two adjacent modules. The design parameters of the robot are listed in Table I. Detailed description of each part is given in the subsequent sections.

A. *Foldable OmniCrawler module*

The OmniCrawler module consists of a couple of chain-sprocket power transmission pairs on both sides of the chassis, each of which is driven by a micro motor to provide driving motion in the forward and backward direction. An exploded view of the CAD model including chains, lugs, motor mounts, bearings, couplers and chassis, to accompany the following description, is shown in Fig. 2. The holonomic motion of the module is characterized by the circular cross-section of the lugs. Two identical longitudinal series of lugs rest on chain links through attachments via fastener, which gives a circular cross-section to the module, shown in Fig. 3, and the ends of the module attain hemispherical shape. The design and arrangement of the module components is done such that the diameter of the lugs is minimum based on size constraints of actuators. The lugs are coated with a layer of latex rubber, to provide sufficient traction for climbing. The sideways rolling motion of each module is realized with an external actuator connected to the module's chassis with a coupler.

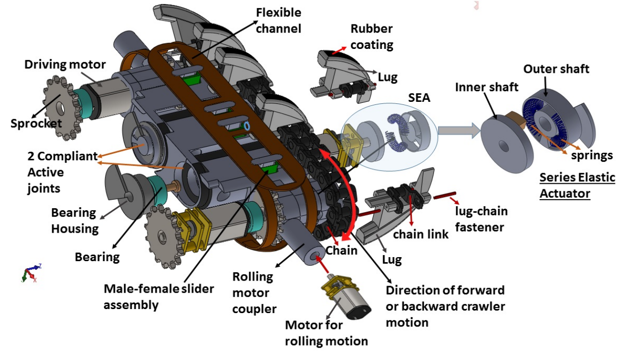

Fig. 2: Exploded view of the module

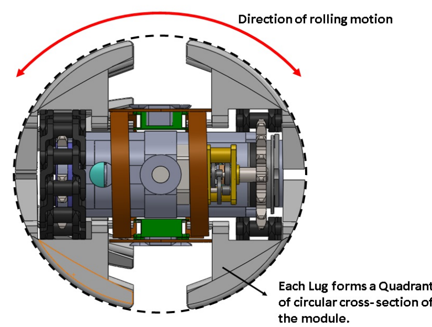

Fig. 3: Cross-sectional view of module.

TABLE I: Design Parameters of the robot

Quantity	Symbol	Values
mass of module	m_m	0.150kg
mass of link	m_l	0.020kg
length of modules	l_1,l_2,l_3	0.14m
Diameter of modules	d	0.050m
length of links	L_1,L_2	0.060m
Diameter of pipe	D	0.065m to 0.1m
Driving motors saturation torque	τ_{max}	1Nm

The OmniCrawler module compliance is realized by incorporating two active hinge joints in the support structure (chassis) of the module. Each such revolute joint is actuated by a geared motor with its shafts connected in series with

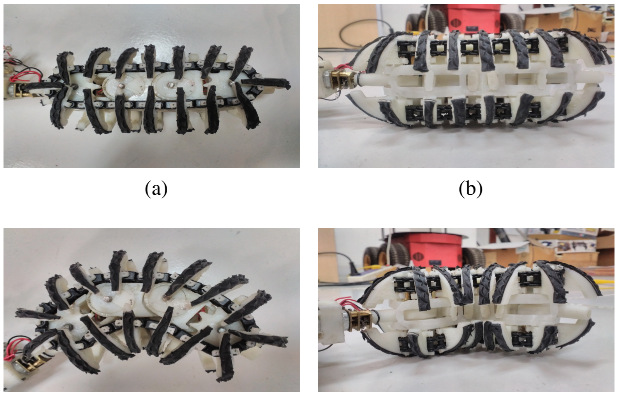

(a) (b) (c) (d)

Fig. 4: (a) Top view of the straight configuration. (b) Side view of the straight configuration. (c) Top view of the bend configuration. (d) Side view of the Bend configuration

(a) (b)

Fig. 5: (a) Rolling Motion about the axis of the pipe, (b) Maximum energy posture (left) and minimal energy posture (right) for turning.

an assembly of dual shafts (inner and outer shaft) and linear springs. The inner shaft is connected to the motor shaft and the outer shaft to the hinge joint. This arrangement of geared motor and the linear springs acts as a series elastic actuator (SEA) [16] and is being used to achieve module compliance. It further filters out vibrations while overcoming jagged terrains during forward propulsion of the robot and thereby, protects the joint motors gears from getting damaged. To ensure that the chains as well as lugs align themselves along the bent chassis, a flexible guiding channel goes over the entire module's body and provides a passage to the lugs-chain assembly. This is achieved with the aid of channel-lug-chain attachments. Furthermore, a series of coupled male-female slider assembly slides through the flexible channel cavity and enables the lug-channel assembly to maintain a constant height above the chassis, throughout. This slider assembly also acts as a stopper and restricts compliant hinge joint rotations beyond its joint angle limits. The straight and bend configurations of the module are shown in Fig.4.

B. Link design

The link assembly is connected between 2 OmniCrawler modules via passive compliant joints. The link length is determined by the desired pipe diameter as well as pipe bend curvature. To overcome sharp 90° bend in a Ø75 mm pipe, the link assembly incorporates rolling motor clamps of the adjoining modules, as well as a pair of torsion springs corresponding to each compliant passive joint.

III. In-pipe locomotion

A. Locomotion mode in straight pipes

In straight pipes, all 3 modules are aligned in-line with the pipe and are driven synchronously to propagate the robot in forward/backward direction. The preloaded torsion spring joints provide the necessary clamping force to overcome robot's own body weight and facilitate slip free driving motion. The alignment of the robot in straight configuration is shown in Fig.5a.

TABLE II: Nomenclature for model description

Symbols	Quantity
k_1, k_2, k_3, k_4	torsion spring constant of 4 passive joints
ij	represents j^{th} sub-module of i^{th} module,
wm_{ij}	weight of ij^{th} sub-module
d	Diameter of the module
l_{ij}	length of sub-module
F_{ij}	Friction force of ij^{th} sub-module
N_{ij}	Normal force acting on ij^{th} sub-module
θ_{ij}	angle of ij^{th} sub-module with global x(horizontal) axis
J_{ij}	represents joint between i^{th} and j^{th} sub-module
wl_k	weight of k^{th} link (k^{th} link connects k^{th} module with $k+1^{th}$ module
L_k	length of k^{th} link
θ_k	angle of k^{th} link with the horizontal axis
D	Diameter of the pipe (represented as Ø)
μ	coefficient of friction
f_x	force acting in x direction
f_y	force acting in y direction
M_J	Moment acting on joint J
τ_k	torque

B. Locomotion mode in bend pipes

In order to overcome pipe turns, the robot aligns itself along the direction of the bend, beforehand. All 3 modules synchronously rolls about their own axes such that their axes continue to remain in the same plane, as shown in Fig.5a, and as a result, the robot rolls about the axis of the pipe. When the robot attains this minimum energy posture where the passive compliant joints apply minimal torque while bending, as shown in Fig.5b, the collaborative control of SEAs of each module enables the robot to comply with the curvature of the pipe. Owing to the lug-chain arrangement, each module can crawl forward in the bend configuration, which propagates the robot forward while complying with the bends.

IV. Optimization Framework

An optimal spring stiffness estimation is critical for providing sufficient clamping force to climb the robot in vertical straight and bend pipes. Lower values of spring stiffness result in insufficient traction and lead to slippage, whereas higher values result in a larger moment at these joints.

A. *Determining Optimal Spring Stiffness*

The estimation of optimal spring stiffness is formulated as an optimization problem with an objective to minimize the sum of torsion spring joint moments, which ensures that the springs are neither too stiff not too relaxed.

$$min \sum_{j=1}^{4} |\tau_j| \tag{1}$$

This function being linear and convex, is guaranteed to converge to a global optima. The constraints posed by the geometry, model as well as motion of the robot to perform this optimization, are discussed in the subsequent sections. All the symbols used for the derivation are defined in Table II.

1) No slip constraint: In order to avoid slippage at robot-pipe surface interface, friction force which directly relates with the wheel torque must satisfy the following constraint.

$$F_{ij} = F_{static} \leq \mu N_{ij}, \forall i, j \in \{1, 2, 3\} \tag{2}$$

Moreover, the maximum traction force is constrained by the driving motor torque limits.

$$F \leq \frac{2\tau_{max}}{(d/2)} \tag{3}$$

To determine these unknown parameters $(N_{ij}, F_{ij}, \tau_{ij})$, we need to formulate a model of the robot to associate all the forces and torques with the spring joint moments. As the robot crawls at a speed of 0.5 m/sec and at such low speed, the motion of a robot is dominated by the surface forces rather than dynamic and inertial effects [14], the slow motion crawling behavior can be well captured by the quasi-static model of the robot, which is discussed in the following section.

2) Quasi-static analysis and Kinematic constraints: For the mathematical analysis, each submodule is modeled as a symmetric Omniball, as proposed by [13].

(i) *In straight configuration*

With the modules aligned in-line with the straight pipes, as shown in Fig.6, the joint angles θ_1, θ_2 are geometrically determined as following.

$$\begin{aligned} \theta_1 &= \pi - cos^{-1}\left(\frac{D-d}{L_1}\right) \\ \theta_2 &= cos^{-1}\left(\frac{D-d}{L_2}\right) \end{aligned} \tag{4}$$

With the posture parameters (θ_1, θ_2), the quasi static model can be obtained by balancing the forces (equation.5 and 6) and joint moments at J_1, J_2, J_3 and J_4 (equations.7-10), as follows.

$$\Sigma f_x = 0, \qquad N_1 - N_2 + N_3 = 0 \tag{5}$$

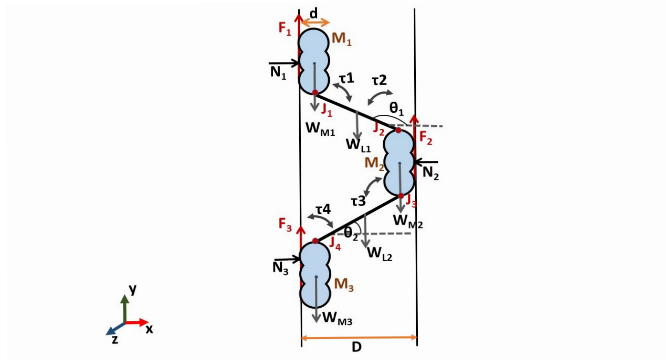

Fig. 6: Quasi-static configuration in vertical straight pipe

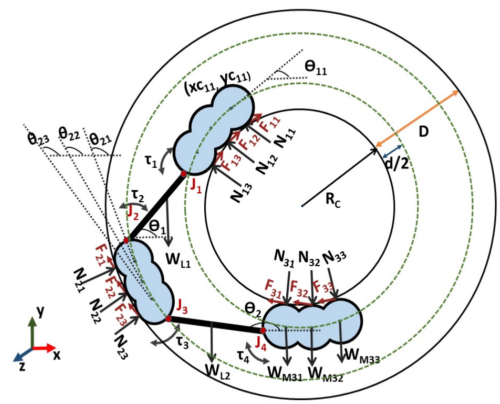

Fig. 7: Quasi-static configuration in vertical bend pipes

$$\Sigma f_y = 0, \qquad \begin{aligned} &F_1 + F_2 + F_3 - wm_1 - wm_2 \\ &- wm_3 - wl_1 - wl_2 = 0 \end{aligned} \tag{6}$$

$$\Sigma M_{J_1} = 0, \qquad F_1 d/2 + N_1 l_1/2 - \tau_1 = 0 \tag{7}$$

$$\Sigma M_{J_2} = 0, \qquad \begin{aligned} &F_1 L_1 \cos\theta_1 + N_1 L_1 \sin\theta_1 - \\ &wm_1 L_1 \cos\theta 1 - wl_1 L_1/2 \cos\theta_1 + \\ &\tau_1 - \tau_2 = 0 \end{aligned} \tag{8}$$

$$\Sigma M_{J_3} = 0, \qquad \begin{aligned} &- F_2 d/2 + N_1 l_1 - N_1 l_2/2 + \\ &\tau_2 - \tau_3 = 0 \end{aligned} \tag{9}$$

$$\Sigma M_{J_4} = 0, \qquad \begin{aligned} &- F_1 L_2 \cos\theta_2 + N_1 L_2 \sin\theta_2 - \\ &F_2 L_2 \cos\theta_2 - N_2 L_2 \sin\theta_2 + \\ &(wm_2 + wm_1 + wl_1) L_2 \cos\theta_2 + \\ &wl_2 (L_2/2)\cos(\theta_2) + \\ &\tau_3 - \tau_4 = 0; \\ &N_3 l_3/2 - F_3 d/2 - \tau_4 = 0 \end{aligned} \tag{10}$$

(ii) *In bend configuration*

The desired posture of the folding Omni-Crawler modules in the bent configuration should comply with the geometry of curvature of the bend pipes,as shown in Fig.7. The joint angles of each submodule corresponding to the desired posture can be geometrically determined, subject to the constraint that the center of all sub-modules must trace a circle of radius R_{cin} or R_{cout}.

$$\begin{aligned} R_{cin} &= R_c + d/2 \\ R_{cout} &= R_c + D - d/2 \end{aligned} \tag{11}$$

$$\begin{aligned} &(xc_{ij} - xc)^2 + (yc_{ij} - yc)^2 = R^2 \quad \forall i, j \\ &R = R_{cin}, \qquad i \in \{1, 3\}, j \in \{1, 2, 3\} \\ &R = R_{cout}, \qquad i \in \{2\}, j \in \{1, 2, 3\} \end{aligned} \tag{12}$$

where,
R_c: radius of curvature of the pipe
(xc_{ij}, yc_{ij}) : coordinates of center of ij_{th} submodule, as shown in Fig.7.

After determining the center of each submodule, their joint angles (θ_{ij}) as well as passive joint angles (θ_k) can be be estimated as below.

$$\begin{gathered} \theta_{ij,k} = tan^{-1}\left(\frac{yc_{ij,k} - yc}{xc_{ij,k} - x_c}\right) - \pi/2 \\ \forall i \in \{1, 2, 3\}, \forall k \in \{1, 2\} \end{gathered} \tag{13}$$

Similar to equations 5-10, a set of equations are derived by balancing the forces and moment in bend configuration. The detailed derivation is uploaded at `http://robotics.iiit.ac.in/Archives/pipe_climbing_robot_quasistatic.pdf`. These equations form the equality constraints and are represented as $Ax = b$, where x is a vector of variables ($x = [(F_{ij})^T, (N_{ij})^T, (\tau_{ij})^T]^T$).
Therefore, the optimization can be formulated as

$$\begin{aligned} &\min_{\tau_j} \sum_{j=1}^{4} |\tau_j| \\ \text{subject to} \quad &Ax = b, \\ &F_{ij} \leq \mu N_{ij}, \quad \forall i, j \in \{1, 2, 3\} \end{aligned} \tag{14}$$

B. Determining the range of friction coefficients for no-slip climbing

In an in-pipe environment, estimation of an exact value of μ for the robot-pipe surface interface is difficult. Moreover, the friction changes dynamically along the pipe networks. Therefore, it is required to analyze the climbing ability of the robot inside pipes with varying friction coefficients. This is achieved by finding a minimum μ of the surface, on which this robot can climb without slippage using spring stiffness values obtained from equation (14). For a given μ, no-slip condition is achieved by maximizing the traction force while climbing. However, this traction force must neither exceed the maximum force that a terrain can bear nor the motor saturation torques, as stated in equations 2 and 3. Therefore, the objective of slippage avoidance can be achieved by minimizing the maximum ratio of traction force (F_{ij}) to the normal force (N_{ij}) [15] at the point of contact of ij^{th} submodule with the surface of the pipe.

$$R = \max\{F_{ij}/N_{ij}\}$$

By minimizing the function R, it is ensured that the required minimum traction force per unit normal force is being applied to maintain static stability, in a particular configuration. However, being a non-linear function, the optimization process may get stuck in local optima and strictly depends on a strong initial guess to converge to a value closer to global optima. Therefore, the objective is modified as maximizing the sum of Normal forces as it eventually minimizes the cost function R.

$$\begin{aligned} &\max_{Fij/Nij} \sum_{i,j} |N_{ij}|^2 \\ \text{subject to,} \quad &Ax = b, \\ &F_{ij} \leq N_{ij}, \quad \forall i, j \in \{1, 2, 3\} \end{aligned} \tag{15}$$

Since, this optimization is carried out with the stiffness values (k_1, k_2, k_3, k_4) determined from solution to equation 14, the variables here include only F and N ($\therefore x = [[F_{ij}]^T, [N_{ij}]^T]^T$).

$$\therefore \qquad \mu_{lim} = \max(F_{ij}/N_{ij})$$

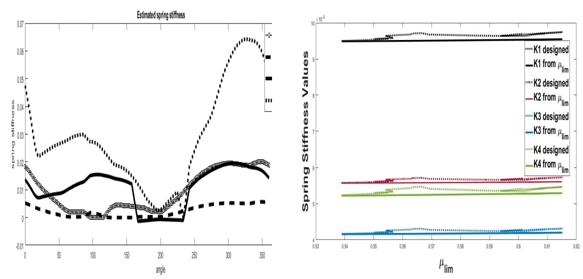

(a) (b)

Fig. 8: Plots obtained from optimization at bends. (a) Springs stiffness values versus ϕ, (b) Springs stiffness corresponding to μ and μ_{lim}

V. Simulation Results

To validate the proof of concept of the design as well as optimize the design parameters for a desirable pipe environment, simulations were carried out with a lumped model of the robot in ADAMS MSC, a multi-body dynamics simulator. With the design parameters listed in Table I, the formulated constrained Optimization (equation.14) yields a minimal set of passive compliant joint torques at J_1, J_2, J_3 and J_4, to statically balance the robot. This is further used to obtain the stiffness values, assuming the springs to be linear.

$$\begin{aligned} &\tau = k(\theta - \theta_{initial}), \\ \text{where,} \quad &k : \text{spring stiffness} \\ &\theta : \text{current joint angle} \\ &\theta_{initial} : \text{initial joint angle (preloaded)} \end{aligned} \tag{16}$$

For vertical straight climbing in Ø75 mm pipes, the joint angle values obtained from equation (4) are $\theta_1 = 115°$ and $\theta_2 = 65°$ and joint moment values are $\tau_{J_1} = 0.2359$ Nm, $\tau_{J_2} = 0.3683$ Nm, $\tau_{J_3} = 0.2760$ Nm, $\tau_{J_4} = 0.1310$ Nm, which gives the following spring stiffness values.
k_1= 0.0096 Nm/deg, k_2 = 0.0056 Nm/deg,
k_3 = 0.0042 Nm/deg, k_4 = 0.0053 Nm/deg

Though the springs stiffness values obtained above were successfully simulated to climb vertical straight pipes, slippage was observed while steering in pipe turns. Therefore, a similar analysis was done for a 360° circular pipe trajectory, as shown in Fig.7, where each quadrant represents one of the possible configurations of a 90° elbow (transition from vertical to horizontal and horizontal to vertical, in both upward and downward directions) in a pipe network.

The circular trajectory was discretized into n(=360) steps and an optimization was carried out $\forall\ l \in [1, n]$. Fig.8a shows a plot for optimal spring stiffness values $\forall l \in [1, n]$. Here, it can be observed that the springs at joints J_3 and J_4 need to be more stiffer to balance the moments due to forces of the adjoining modules and links, which can also be illustrated from quasi-static equations. The pattern also shows that the stiffness values k_1, k_2, k_3 and k_4 are consistent for $\forall \phi \in [0, 150°]$ and therefore, the spring stiffness values were selected as the maximum within this range of ϕ. The obtained values are listed below.
k_1 = 0.0262 Nm/deg, k_2 = 0.0170 Nm/deg,
k_3 = 0.0163 Nm/deg, k_4 = 0.0232 Nm/deg

These values were further successfully verified in simulation for 90° bends in a Ø75 mm pipes. However, the sudden increase in the stiffness value k_4 at $\phi = 320°$, in Fig.8a, shows that the horizontal to vertically upward climbing via a $\phi = 90°$ elbow could not be addressed by these values.

In addition to above, the springs' stiffness values obtained for vertical climbing were further used to estimate μ_{lim} (from equation 15). The F/N ratio obtained for modules $M1, M2$ and $M3$ are 0.5180, 0.4629 and 0.5054, respectively. Therefore,

$$\mu_{lim} = max(0.5180, 0.4629, 05.5054) = 0.5180$$

This implies that with the available driving motor saturation torques, the robot is able to successfully climb in vertical pipes with $\mu_{lim} < \mu < 1$, with the designed springs. This μ_{lim} was further used to obtain spring stiffness values from Optimization (equation.14). Fig.8b shows two curves for each k_1, k_2, k_3, k_4 representing the difference in the stiffness values obtained for a μ and μ_{lim}. The difference indicates that the spring was designed for a particular μ and is able to work well with μ_{lim}, by exploiting the driving motor torques well to its saturation limits.

VI. Experiments

Extensive experiments were conducted to validate the numerical and simulation results of the proposed design. The robot was manually controlled by an operator. The initial prototype was developed with non-compliant modules with the optimal spring stiffness values. This could successfully climb vertical pipes, as demonstrated in Fig.9. However, it could not negotiate Ø75 mm smooth elbows because of its diametric non-uniformity along the bends. This issue could be further solved by incorporating an active compliant joint in the module, which would successfully overcome sharp 45° turns. However, this design was not realized in practice since sharp 90° turn still remained unaddressed as the active compliance joint angle limit is 40°. This led to the design of a module with 2 active compliant joints, each with a joint angle limit of 35° and all further experiments were performed using this prototype. The experimental results demonstrating the traversal of the robot in 90° and 45° sharp elbow are shown in Fig. 10a and 10b, respectively. In order to align the robot in the direction of bend, Fig. 10c shows the rolling motion about the axis of the pipe, followed by steering in the turn.

Subsequently, the vertical climbing was successfully tested in a pipe with a glossy paper on its surface, to validate the climbing ability in the limiting friction coefficient surface. Fig. 9 shows the vertical climbing in pipes with acrylic and glossy surface. All simulation and experimental results are presented in the accompanying video.

(a) (b)

Fig. 9: (a) shows vertical climbing in acrylic pipe (μ=0.7); (b) in glossy paper surface (μ=0.55)

VII. Conclusion and Future Work

In this paper, we discuss the design of a novel compliant OmniCrawler modular robot in-pipeline robot. A combination of modularity, compliance, holonomic motion and good traction enables it to traverse small diameter, smooth and complex pipe networks. For a given pipe environment, a set of optimal spring stiffness values were calculated to quasi-statically balance the robot in straight as well as bend pipes. Afterwards, the limiting value of friction coefficient which could be climbed by the robot without slippage, was calculated. However, the compliant active joint has 1 DOF, which restricts the bending in one direction. This

(a)

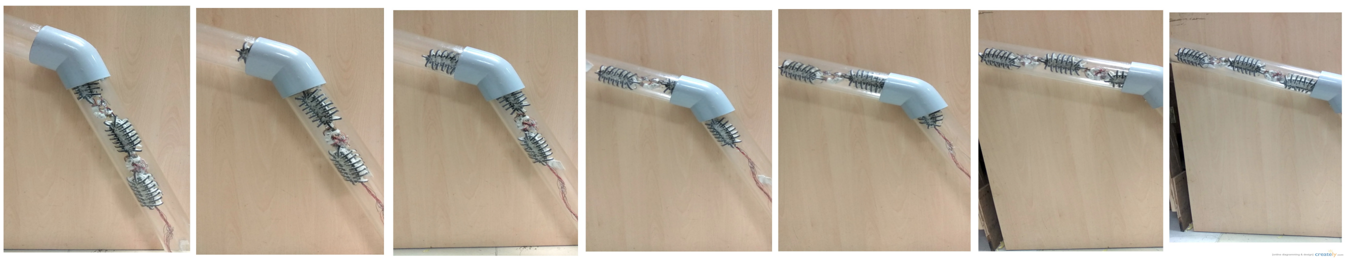

(b)

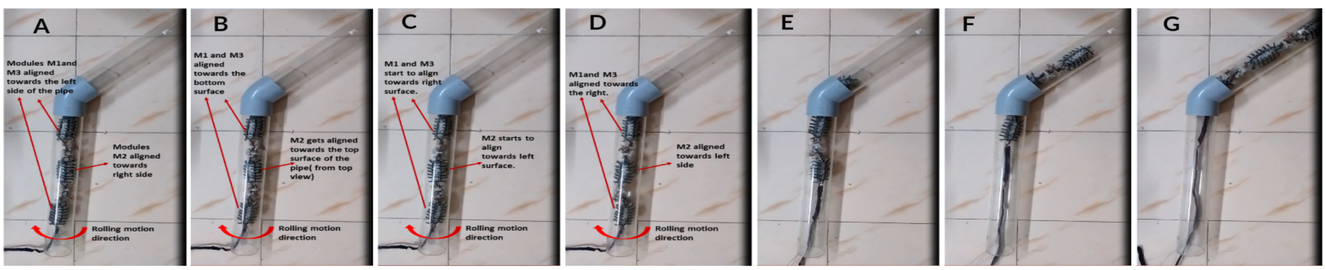

(c)

Fig. 10: Experiments showing traversal in sharp turns. (a) 90° elbow. (b) 45° elbow. (c) Robot aligns itself along 45° turn.

requires robot to attain a configuration corresponding to that direction. Therefore, our future work would focus on modification of the design to bend each module in all directions. Furthermore, a torque control strategy for SEA to comply with diameter and friction coefficient variation would be implemented.

REFERENCES

[1] Roslin, Nur Shahida, et al. "A review: hybrid locomotion of in-pipe inspection robot." Procedia Engineering 41 (2012): 1456-1462.

[2] Dertien, Edwin, et al. "Design of a robot for in-pipe inspection using omnidirectional wheels and active stabilization." Robotics and Automation (ICRA), 2014 IEEE International Conference on. IEEE, 2014.

[3] Debenest, Paulo, Michele Guarnieri, and Shigeo Hirose. "PipeTron series-Robots for pipe inspection." Applied Robotics for the Power Industry (CARPI), 2014 3rd International Conference on. IEEE, 2014.

[4] Roh, Se-gon, et al. "Modularized in-pipe robot capable of selective navigation inside of pipelines." Intelligent Robots and Systems, 2008. IROS 2008. IEEE/RSJ International Conference on. IEEE, 2008.

[5] Choi, Hyouk Ryeol, and Se-gon Roh. In-pipe robot with active steering capability for moving inside of pipelines. INTECH Open Access Publisher, 2007.

[6] Roh, Se-gon, and Hyouk Ryeol Choi. "Differential-drive in-pipe robot for moving inside urban gas pipelines." IEEE transactions on robotics 21.1 (2005): 1-17.

[7] Kakogawa, Atsushi, and Shugen Ma. "Design of a multilink-articulated wheeled inspection robot for winding pipelines: AIRo-II." Intelligent Robots and Systems (IROS), 2016 IEEE/RSJ International Conference on. IEEE, 2016.

[8] Hirose, Shigeo, et al. "Design of in-pipe inspection vehicles for/spl phi/25,/spl phi/50,/spl phi/150 pipes." Robotics and Automation, 1999. Proceedings. 1999 IEEE International Conference on. Vol. 3. IEEE, 1999.

[9] Kakogawa, Atsushi, Taiki Nishimura, and Shugen Ma. "Development of a screw drive in-pipe robot for passing through bent and branch pipes." Robotics (ISR), 2013 44th International Symposium on. IEEE, 2013.

[10] Roh, Se-gon, et al. "In-pipe robot based on selective drive mechanism." International Journal of Control, Automation and Systems 7.1 (2009): 105-112.

[11] Kwon, Young-Sik, and Byung-Ju Yi. "Design and motion planning of a two-module collaborative indoor pipeline inspection robot." IEEE Transactions on Robotics 28.3 (2012): 681-696.

[12] Kakogawa, Atsushi, and Shugen Ma. "Design of an underactuated parallelogram crawler module for an in-pipe robot." Robotics and Biomimetics (ROBIO), 2013 IEEE International Conference on. IEEE, 2013.

[13] Tadakuma, Kenjiro, et al. "Crawler mechanism with circular section to realize a sideling motion." Proceeding of IEEE/RSJ International Conference on Intelligent Robots and Systems Acropolis Convention Center. Nice, 2008.

[14] Qian, Feifei, et al. "Walking and running on yielding and fluidizing ground." (2012): 345-352.

[15] Iagnemma, Karl, et al. "Planning and control algorithms for enhanced rough-terrain rover mobility." International Symposium on Artificial Intelligence, Robotics, and Automation in Space. Vol. 2. No. 2. 2001.

[16] Pratt, Gill A., and Matthew M. Williamson. "Series elastic actuators." Intelligent Robots and Systems 95.'Human Robot Interaction and Cooperative Robots', Proceedings. 1995 IEEE/RSJ International Conference on. Vol. 1. IEEE, 1995.